Biogeosciences
Discussions

1 **Spatiotemporal transformation of dissolved organic matter along an alpine stream**

2 **flowpath on the Qinghai-Tibetan Plateau: importance of source and permafrost**

3 **degradation**

4

5 Yinghui Wang [a,b], Robert G.M. Spencer [c], David Podgorski [d], Anne Kellerman [c],

6 Harunur Rashid [a], Phoebe Zito [d], Wenjie Xiao [b], Dandan Wei [a], Yuanhe Yang [e], Yunping

7 Xu [a*]

8 [a] *Shanghai Engineering Research Center of Hadal Science and Technology, College of Marine*

9 *Sciences, Shanghai Ocean University, Shanghai 201306, China.*

10 [b] *Key Laboratory for Earth Surface Processes of the Ministry of Education, College of Urban and*

11 *Environmental Sciences, Peking University, Beijing 100871, China.*

12 [c] *National High Magnetic Field Laboratory Geochemistry Group and Department of Earth, Ocean,*

13 *and Atmospheric Science, Florida State University, Tallahassee, FL 32306, USA*

14 [d] *Pontchartrain Institute for Environmental Sciences, Department of Chemistry, University of New*

15 *Orleans, New Orleans, LA, 70148, USA*

16 [e] *State Key Laboratory of Vegetation and Environmental Change, Institute of Botany, Chinese*

17 *Academy of Sciences, Beijing 100093, China*

18 *Corresponding author. E-mail: ypxu@shou.edu.cn (Y. Xu)

19

Biogeosciences

Discussions

Open Access

EGU

20 **Abstract** The Qinghai-Tibetan Plateau (QTP) accounts for approximately 70% of

21 global alpine permafrost and is an area sensitive to climate change. The thawing and

22 mobilization of ice and organic carbon-rich permafrost impact hydrologic conditions

23 and biogeochemical processes on the QTP. Despite numerous studies of Arctic

24 permafrost, there are no reports to date for the molecular-level in-stream processing of

25 permafrost-derived dissolved organic matter (DOM) on the QTP. In this study, we

26 examine temporal and spatial changes of chemical composition of DOM and ^{14}C age

27 of dissolved organic carbon (DOC) along an alpine stream (3850–3207 m above sea

28 level) by Fourier transform ion cyclotron resonance mass spectrometry (FT-ICR MS),

29 accelerator mass spectrometry (AMS) and UV-visible spectroscopy. Compared to

30 downstream sites, the DOM at the headstream exhibited older radiocarbon (^{14}C-DOC)

31 age, higher mean molecular weight, higher aromaticity and fewer polyunsaturated

32 components. At the molecular level, 6409 and 1345 formulas were identified as unique

33 to the active layer (AL) leachate and permafrost layer (PL) leachate, respectively.

34 Comparing permafrost leachates to the downstream site, 59% of AL-specific formulas

35 and 90% of PL-specific formulas were degraded, likely a result of rapid instream

36 degradation of permafrost-derived DOM. From peak discharge in the summer to low

37 flow in late autumn, the DOC concentration at the headstream site decreased from 13.9

38 to 10.2 mg/L, while the ^{14}C-DOC age increased from 745 to 1560 years before present

39 (BP), reflecting an increase in relative contribution of deep permafrost carbon due to

40 the effect of changing hydrological conditions over the course of the summer on DOM

41 source (AL vs. PL). Our study thus demonstrates that hydrological conditions impact

42 the mobilization of permafrost carbon in an alpine fluvial network, the signature of

43 which is quickly lost through in-stream metabolism.

44 Keywords: dissolved organic matter; permafrost; Qinghai-Tibet Plateau; FT-ICR MS;

Biogeosciences
Discussions

Open Access

EGU

45   radiocarbon age

46

47   **1. INTRODUCTION**

48   The amount of carbon stored in permafrost is roughly twice as much as that in the

49   atmosphere and represents the largest component of the terrestrial carbon pool (Zimov

50   et al., 2006; Tarnocai et al., 2009). Accelerated climate warming has led to a succession

51   of changes associated with permafrost thaw, where liquid water once frozen in

52   permafrost soils has changed watershed hydrology, topography and ecosystem

53   biogeochemistry (Frey and Smith, 2005; Abbott et al., 2015; Vonk et al., 2015). When

54   permafrost-derived carbon enters aquatic systems, it can be rapidly bio- and photo-

55   degraded (Cory et al., 2014; Drake et al., 2015; Vonk et al., 2015). Therefore, the

56   mobilization of carbon from permafrost soils where it has been relatively stable for

57   thousands of years into dissolved carbon could increase greenhouse gas emissions

58   (Cory et al., 2013; Vonk et al., 2013; Mann et al., 2015; Ward and Cory, 2016; Selvam

59   et al., 2017) and exacerbate climate warming via a positive feedback loop (Koven et al.,

60   2011; Schuur et al., 2015).

61   The seasonal thawing-freezing cycle of permafrost soils could change hydrologic

62   inputs and restrict source water contributions to river flow, leading to variability in the

63   flux and the chemical composition of dissolved organic matter (DOM) in permafrost-

64   impacted watersheds (Petrone et al., 2006; Laudon et al., 2011). DOM in the Yukon

65   River exhibits seasonal changes in aromaticity, molecular weight, ^{14}C age and

66   biodegradability (Striegl et al., 2007; Spencer et al., 2008; Wickland et al., 2012;

67   O'Donnell et al., 2014). Since the persistence of DOM in aquatic systems is related to

68   chemical composition (Kellerman et al., 2015; Kellerman et al., 2018), substituting

69   space for time to trace changes in DOM composition along a hydrologic flowpath may

70   illustrate the environmental behavior and fate of seasonally exported permafrost carbon.

71   The Qinghai-Tibet Plateau (QTP), the world's largest and highest plateau, plays a

72   critical role in the evolution of the Asian Monsoon (Sato and Kimura, 2007; Wu et al.,

73   2007) and supplies water to several large rivers such as the Yangtze River, Yellow River

74   and Yarlung Tsangpo (Yao et al., 2007; Kang et al., 2010). As a climate sensitive region,

75   the QTP has experienced significant warming since the 1950s (Qiu, 2008) with the

76   mean annual air temperature rising at a rate of 0.36 °C per decade from 1961 to 2007

77   (Wang et al., 2008). Consequently, the permafrost soils on the QTP have begun to thaw

78   and collapse, causing abundant carbon loss from degradation, leaching and lateral

79   displacement (Mu et al., 2016). However, compared with an abundance of studies on

80   Arctic permafrost, biogeochemical studies on QTP permafrost are scant (Mu et al.,

81   2016). This results in a limited understanding of the permafrost carbon cycle as a whole

82   since the QTP represents nearly 10% of the global permafrost, what's more, the QTP

83   differs from the Arctic in altitude, climate, and hydrology (Bockheim and Munroe,

84   2014).

85   Here, we conducted a study on the spatial and temporal change of permafrost-derived

86   DOM on the northeastern QTP. We applied multiple analytical techniques including

87   Fourier transform ion cyclotron resonance mass spectrometry (FT-ICR MS), AMS

88   radiocarbon (^{14}C), and UV-visible optical spectroscopy. Our objective is two-fold: 1)

89   determine the dominant sources of alpine stream DOM on the QTP (active layer (AL)

90   vs. permafrost layer (PL)), and 2) trace the persistence and degradation of permafrost-

91   derived DOM in an alpine fluvial network. This work represents the first step in

92   characterizing in-stream removal and transformation processes of permafrost carbon at

93   the molecular level on the QTP.

94

2. MATERIALS AND METHODS

2.1. Study area and sampling

Our study area is located in Gangcha County, north of Qinghai Lake. The climate is typical plateau continental climate, characterized by extensive sunshine duration (~3000 hours per year), long cold and dry winters and short cool and humid summers (Peng et al., 2015). During 2013-2016, January had the lowest average monthly temperature (–11.82 °C), while December had the lowest average monthly precipitation (0.3 mm). Meanwhile, the highest average monthly temperature and precipitation occurred in July (11.66 °C) and August (124.67 mm), respectively. These climate data are available at http://data.cma.cn. The permafrost soil was developed in the late Quaternary, and accumulated > 2 m thick in mountainous areas of the Gangcha County. Due to the rapid climate warming on the QTP, the ice-rich permafrost began to thaw, and several thermo-erosion gullies formed a decade ago. In this study, we focused on a continuous system that starts with a thermo-erosion gully (> 200 m long), forms a stream which flows into Qinghai Lake, the largest lake in China with a surface area of ca. 4500 km^2. Thawed permafrost slumping exposed soil profiles at the gullies' head (ca. 3850 meters above sea level; masl). The top 60 cm is an active layer (AL) that comprises abundant grass litter and roots, underlain by a dark permafrost layer (PL) without visible plant debris. The thaw depth reached 78 cm in August 2015. Seasonal thaw of the entire AL and the upper PL allows for both vertical and lateral percolation of rainwater, which mobilizes large amounts of particulate and dissolved organic matter. The water in the gully flows southward across the hillslope before draining into Qinghai Lake (3196 masl; Fig. 1).

Our fieldwork was conducted in the summer and autumn of 2015 and 2016. In 2015, a time-series sampling campaign was conducted at the headstream (Q-1) from August

120   1st when the warm and humid climate caused the largest export of leachates, to October

121   15th when the leaching ceased due to little precipitation and low temperature. The AL

122   and PL leachate samples were collected at a depth of 60 cm and 220 cm, respectively,

123   at the gullies' head. For each leachate sample, >15 L water was gathered over 2 days

124   using a 20 L pre-cleaned HDPE carboy. Besides soil leachates, water samples (20 L

125   each) were collected from twenty sites along the stream (Fig. 1). Sampling sites Q-1 to

126   Q-10 are located in a first-order stream that originates in the largest thermo-erosion

127   gully, whereas sites Q-11 and Q-12 are located in another first-order stream nearby.

128   These two streams merge together to form the main stream, along which sampling sites

129   Q-13 to Q-20 were located. Surface water samples were collected using pre-cleaned

130   HDPE carboys and kept on ice and in the dark until filtering through Whatman GF/F

131   filters (0.7 µm) within 6 hours after sampling. To obtain enough carbon for ^{14}C analyses,

132   aliquots of the 0.7 µm filtrate were concentrated over a cross-flow ultrafiltration system

133   with 1 kDa cut off (Millipore®, Pellicon 2 system). The retentates and the remaining

134   filtrate were all stored at –20 $^{\circ}$C until further analysis. All glassware and GF/F filters

135   were combusted at 450 $^{\circ}$C for at least 4 hours prior to use.

136

137   **2.2. Hydrological condition, DOC concentration and spectral absorbance in alpine**

138   **streams**

139   On Aug. 1st 2015, stream water temperature, pH and conductivity were measured

140   with a portable Horiba W-23XD Water Quality Monitoring System. The water flux was

141   calculated according to flow rate and cross-sectional area of the stream. The DOC

142   concentration of each water sample was determined by 3-5 injections on a Shimadzu

143   TOC-V$_{CPH}$ analyzer using high temperature combustion, and the coefficient of variance

144   across measurements was < 2%.

145   The optical properties of the water samples were determined using a Shimadzu UV-

146   1800 spectrophotometer. The scan range was between 200 and 800 nm and Milli-Q

147   water (18.2 MΩ cm^{-1}) was used as the blank. A quartz cell with 1.0 cm path length was

148   used. The spectral slope of the 275–295 nm region ($S_{275-295}$), an indicator for the

149   molecular weight of DOM (Helms et al., 2008), was determined by applying log linear

150   fits across the wavelengths 275-295 nm. Specific UV absorbance (SUVA$_{254}$), an

151   indicator for relative aromatic C content, was calculated by dividing the decadic UV

152   absorbance at 254 nm with DOC concentration (Weishaar et al., 2003).

153

154   **2.3. Electrospray ionization Fourier transform ion cyclotron resonance mass**

155   **spectrometry (ESI FT-ICR MS)**

156   Selected water samples collected in 2016 from headstream (Q-1), mid-stream (Q-9),

157   and downstream (Q-17), as well as leachate samples collected from the AL and PL,

158   were prepared for FT-ICR MS analyses. They were solid phase extracted (SPE) using

159   the Bond Elut PPL (Agilent Technologies) following the procedures of Dittmar et al.

160   (2008). The aliquot volume of SPE DOM was adjusted for a target final eluate

161   concentration of 40 μg C/ml (in methanol) to aid ionization in negative mode

162   electrospray ionization (ESI). The methanol extracts were analyzed on a 9.4 Tesla

163   custom-built FT-ICR MS at the National High Magnetic Field Laboratory (NHMFL;

164   Tallahassee, FL; Kaiser et al., 2011). The injection speed was 0.7 μL/min. A total of 100

165   broadband scans was accumulated for each mass spectra. Other instrumental parameters

166   can be found in Hodgkins et al. (2016). After internal calibration in MIDAS Predator

167   Analysis (NHMFL), formulas were assigned based on published rules to peaks with

168   intensities > 6σ baseline noise (Stubbins et al., 2010) using EnviroOrg®™ software and

169   categorized by compound class based on the elemental composition of molecular

170   formulas (Spencer et al., 2014; Corilo, 2015). A modified aromaticity index (AI_{mod}) was

171   calculated according to the definition of Koch and Dittmar (2006): $AI_{mod} =$

172    $\frac{1+C-0.5O-S-0.5H}{C-0.5O-S-N}$, and if AI_{mod} is negative, then AI=0. The groups referenced in this study

173   are: 1) aliphatics (Ali.): H/C 1.5 - 2.0, O/C < 0.9, N = 0; 2) peptides (Pep.): H/C 1.5 -

174   2.0, O/C < 0.9, N > 0; 3) highly unsaturated compounds (Uns.): AI_{mod} < 0.5, H/C < 1.5;

175   4) polyphenols (Pol.): 0.5 < AI_{mod} < 0.67; 5) condensed aromatics (CA): $AI_{mod} \geq 0.67$.

176   The relative abundance of the defined compound class was weighted by signal

177   magnitude in each spectrum.

178

179   **2.4. Radiocarbon analyses**

180   Freeze-dried retentates were fumigated with concentrated hydrochloric acid (12 M)

181   in order to remove inorganic carbon. After that, the samples were analyzed on the Keck

182   Carbon Cycle Accelerator Mass Spectrometry (AMS) Facility at the University of

183   California, Irvine, USA. Processing blank and sample preparation backgrounds were

184   subtracted. Radiocarbon concentrations are given as conventional ^{14}C age following

185   Stuiver and Reimer (1993).

186

187   **3. RESULTS**

188   **3.1. Hydrology and DOC concentration from headstream to downstream water**

189   Discharge increased along the stream reach, from 0.15 m^3/min at the headstream

190   (Q-1) on August 1st 2015 to 24.14 m^3/min (Q-19) (Fig. 2). pH increased from 7.4 at Q-

191   1 to 8.2 at Q-4 and remained elevated in the middle and lower stream (7.9 to 8.4).

192   Conductivity was relatively constant from Q-1 to Q-6 (35 to 38 µs/cm), then increased

193   at Q-7 and remained elevated downstream (48 to 60 µs/cm). The DOC concentration

194   was high in headstream waters (e.g., 11.7 ± 0.9 mg/L at Q-1 and 10.2 ± 1.5 mg/L at Q-

195   2; mean ± SD, same hereafter) and decreased downstream (2.5 to 5.8 mg/L from Q-5

196   to Q-20). The mean DOC concentration of the AL leachates (11.6 ± 1.1 mg/L) was an

197   order of magnitude lower than that of the PL leachates (126.4 ± 20.9 mg/L).

198

199   **3.2. Optical properties of DOM in leachates and stream waters**

200   The mean $S_{275-295}$ was (14.5 ± 0.48) × 10^{-3} nm^{-1} for the AL leachates and (18.3 ±

201   1.3) × 10^{-3} nm^{-1} for the PL leachates. In the stream waters, the $S_{275-295}$ ranged from 15.8×

202   10^{-3} to 22.5 × 10^{-3} nm^{-1}, increasing in downstream reaches. SUVA$_{254}$ was 3.52 ± 0.24 L

203   mg C^{-1} m^{-1} for the AL leachates and 0.95 ± 0.14 L mg C^{-1} m^{-1} for the PL leachates, and

204   decreased in the stream from Q-1 to Q-10 (3.06 to 1.27 L mg C^{-1} m^{-1}), and then remained

205   low (Fig. 3). A strong negative correlation was found between SUVA$_{254}$ and $S_{275-295}$ for

206   water samples from both years (R^2 = 0.77, P < 0.01). Neither stream waters nor

207   permafrost leachates show an interannual variation of optical properties (Fig. 3).

208

209   **3.3. Spatiotemporal change of ^{14}C-DOC age through fluvial networks**

210   ^{14}C-DOC age of the PL leachate was 4145 years BP, which was much older than

211   that of the AL leachate (535 years BP; Fig. 4a). The ^{14}C-DOC age decreased along the

212   stream from 745 years BP for the headstream water (Q-1) to 160 years BP at Q-19, a

213   site close to Qinghai Lake. Besides apparent spatial variability, the ^{14}C-DOC age also

214   changed temporally. In 2015, the ^{14}C-DOC age of the headstream water (Q-1) increased

215   from 745 years BP on August 1st, to 1015 years BP on August 11th and 1560 years BP

216   on September 5th (Fig. 4b).

217

218   **3.4. FT-ICR MS characterization of SPE-DOM**

219   Compared with the PL leachate, the AL leachate was characterized by higher

Biogeosciences Open Access

EGU

Discussions

220   molecular richness (14709 vs. 9645 assigned formulae), higher mean molecular weight

221   (498.81 vs. 452.73 Da) and higher AI_{mod} (0.47 vs. 0.30). Elemental composition

222   revealed that compounds containing both N and S were only detected in the AL

223   leachates and headstream waters. The AL leachate contained 54.28% highly unsaturated

224   compounds, 27.10% polyphenols and 17.23% condensed aromatic compounds,

225   whereas the proportion of aliphatics and peptides was minor (ca. 1.30%). Compared

226   with the AL leachate, the PL leachate comprised a higher proportion of polyunsaturated

227   compounds (74.23%) and aliphatics + peptides (10.04%), but a lower proportion of

228   polyphenols (11.33%) and condensed aromatics (4.32%).

229

230   Along the stream (Q-1, Q-9, and Q-17), the molecular richness, mean molecular

231   weight and modified aromaticity index of SPE-DOM decreased by 26% (14924 to

232   11074), 4.7% (510.1 to 486.5 Da), and 16.3% (0.43 to 0.36), respectively (Table 1). The

233   relative abundance of aromatics (condensed aromatics and polyphenols) decreased by

234   48% (35.7% at Q-1 vs. 18.4% at Q-17), whereas that of highly unsaturated compounds

235   increased by 28% (62.8% at Q-1 vs. 80.3% at Q-17). Aliphatics and peptides were

236   minor components of stream DOM (<1.3%) and did not exhibit a downstream trend.

237

238   **4. DISSCUSSION**

239   **4.1. AL leachates as a major source of stream DOM**

240   The UV-visible optical parameters and molecular formulas resolved by FT-ICR MS

241   show that the AL and PL leachates have different chemical compositions (Table 1 and

242   2). Since chemical composition impacts the reactivity of DOM (Kellerman et al., 2015),

243   the differing chemical composition between the AL and PL leachates that enter the

244   stream may influence bioavailability (Vonk et al., 2013) and photolability (Stubbins et

245   al., 2017). Thus, distinguishing DOM source is crucial for understanding in-stream

246   biogeochemical processes in permafrost-impacted systems. DOM may originate from

247   a variety of sources including permafrost soil (AL and PL) leaching, in-situ microbial

248   production, and wet deposition from snow and rain. At the headstream site (Q-1),

249   however, the dominant source of DOM is permafrost soil leaching, as short residence

250   times at the gully head restrict in-stream production and wet deposition is likely

251   negligible due to low DOC concentrations in Tibetan glaciers (0.2-3.3 μg/ml; Spencer

252   et al., 2014). Assuming that headstream DOM is derived only from permafrost soil

253   leaching, we are able to estimate the relative contributions of DOM from the AL and

254   PL.

255   The DOC concentration of the AL leachate (ca. 11.6 ± 1.1 mg/L; mean $\pm$ SD based

256   on samples from 2015 and 2016, n = 2; same hereafter) is similar to that of the

257   headstream (Q-1; ca. 11.7 ± 0.9 mg/L), but substantially lower than that of the PL

258   leachates (ca. 126.4 ± 20.9 mg/L), supporting a predominance of AL-leachate DOM in

259   stream waters. In addition, the $SUVA_{254}$ is 3.51 ± 0.24 L mg C^{-1} m^{-1} for AL leachates

260   (and 0.95 ± 0.14 L mg C^{-1} m^{-1} for PL leachates, whereas the $S_{275-295}$ is $(14.5 \pm 0.48) \times$

261   10^{-3} nm^{-1} for AL leachates and $(18.0 \pm 1.33) \times 10^{-3}$ nm^{-1} for PL leachates. Similar optical

262   properties and DOC concentrations between AL-leachates and the headstream water

263   $(16.5 \pm 0.40 \times 10^{-3}$ nm^{-1} for $S_{275-295}$ and 2.92 ± 0.19 L mg C^{-1} m^{-1} for $SUVA_{254})$ support

264   DOM that leaches from the AL dominates stream DOM. Furthermore, the stream water

265   at Q-1 has a ^{14}C-DOC age of 745 years BP, close to that of the AL leachate (535 years

266   BP), and much younger than that of the PL leachate (4145 years BP). We estimate the

267   portion of AL and PL-derived C by using a binary mixing model based on Δ^{14}C values

268   of bulk DOC (Criss, 1999):

269   $\Delta^{14}C_{DOM} = f_{AL} \times \Delta^{14}C_{AL} + f_{PL} \times \Delta^{14}C_{PL}$

270   $1.0 = f_{AL} + f_{PL}$

Biogeosciences

Discussions

Open Access

EGU

271   According to this model, ca. 94% of DOC collected from stream site Q-1 on Aug.

272   1, 2015 originated from the AL (Fig. 6a). Headstream ^{14}C-DOC age increased from

273   summer to fall (Fig. 4b), reflecting an enhanced contribution of old carbon from the

274   deeper soils (i.e., PL), however, the AL still accounted for ≥ 72% of total DOC exported

275   (Fig. 6a). This binary mixing model may overestimate the contribution of AL to stream

276   DOC since PL-derived DOC may be degraded faster than AL-derived DOC, due to the

277   high biolability of ancient permafrost carbon as shown in Arctic ecosystems (Vonk et

278   al., 2013). Nonetheless, the AL appears as a major contributor to stream DOC in the

279   QTP.

280   Seasonal variation of ^{14}C-DOC (Fig. 4b) has been previously observed in high

281   latitude permafrost areas in Alaska (Aiken et al., 2014; O'Donnell et al., 2014), with the

282   most enriched ^{14}C values observed in the spring and becoming more depleted through

283   summer-fall and/or during winter. The mean monthly air temperature of Gangcha

284   County, after reaching the maximum in July (ca. 10.5 $^{\circ}$C), decreases to 2.1 $^{\circ}$C in

285   September (data from http://data.cma.cn). As air temperature drops, surface soils freeze

286   earlier than deeper soils, leading to an increase in the relative contribution of deep soil

287   carbon (i.e. PL) to stream DOM, although the DOC concentration in Q-1 decreased

288   from 13.9 mg/L to 10.2 mg/L (Fig. 6b).

289

290   **4.2. Selective removal of DOM along the alpine stream on the QTP**

291   The DOC concentration decreased (12.3 to 4.0 mg/L) from upper to mid-stream

292   (Q-1 to Q-5), which could be attributed to a dilution effect and/or in-stream degradation

293   of DOM. Dilution from groundwater is likely since groundwater discharge sustains

294   baseflow of rivers and streams in the QTP (Ge et al., 2008). Downstream groundwater

295   inputs were further supported by the order of magnitude increase in discharge (1.49 to

296   24.14 m^3/min) and increase in conductivity (37 to 60 µs/cm). Moreover, downstream

297   DOC concentrations remained about 3.0-4.0 mg/L (Q-15 to Q-20), indicative of the low

298   DOC concentrations of groundwater. Conversely, a tributary that originated from

299   another thermo-erosion gully merged into the study stream, however, the different

300   tributaries exhibited similar DOC concentrations (e.g., Q-9 and Q-10 vs. Q-11 and Q-

301   12; Fig. 2d). The similarities in DOC concentrations were attributed to homogeneity in

302   dominant vegetation, soil type and climate, and thus, homogeneity in DOM inputs to

303   the different tributaries in our study area. Therefore, additional tributaries could not

304   explain the spatial pattern of DOC concentration.

305   Despite evident dilution, DOC attenuation could be partly due to in-stream

306   degradation given several lines of evidence from optical properties, radiocarbon age

307   and molecular composition. The UV-visible optical parameters, $S_{275-295}$ and SUVA$_{254}$,

308   have been widely used to reveal mean molecular weight and aromaticity of DOM,

309   respectively (Weishaar et al., 2003; Helms et al., 2008; Spencer et al., 2009; Mann et

310   al., 2012). In our study, the $S_{275-295}$ of stream waters varied from 15.8×10^{-3} to $22.5 \times$

311   10^{-3} nm^{-1} (Fig. 3a), comparable to typical riverine DOM values (13.19×10^{-3} to 22.96

312    $\times 10^{-3}$ nm^{-1}), but much lower than that of DOM from continental shelf and slope (29.7

313    $\times 10^{-3}$ to 48.5×10^{-3}nm^{-1}) (Fichot and Benner, 2012), suggesting a moderate degradation

314   of stream DOM on the QTP. A downstream increase for $S_{275-295}$ regardless of sampling

315   time (Fig. 3a) reflects selected degradation of high molecular weight compounds,

316   leading to the enrichment of low molecular weight DOM. This spatial trend is in

317   accordance with the size-reactivity continuum model (Amon and Benner, 1996) that the

318   bioreactivity of DOM decreases along a continuum of size (from large to small). In

319   addition to $S_{275-295}$, SUVA$_{254}$ varied from 1.27 to 3.06 L mg C^{-1} m^{-1}, showing a general

320   decrease downstream (Fig. 3b). Lignin, an aromatic biopolymer specific for vascular

321   plants (Hedges et al., 1997), is relatively resistant to biodegradation (Hedges et al.,

322   1985), but highly photo-labile (Lanzalunga and Bietti, 2000). Cory et al. (2014) found

323   that sunlight accounts for 70% to 95% of water column carbon processing in Arctic

324   rivers and lakes. Given strong solar radiation and long sunshine duration (~3000 hours

325   per year) on the QTP (Peng et al., 2015), photo-degradation could be an important

326   pathway for carbon removal in QTP streams. A strong negative correlation between

327    $S_{275\text{-}295}$ and $SUVA_{254}$ ($R^2 = 0.73$, $p < 0.01$) indicates that photodegradation of high

328   molecular weight aromatic compounds (like lignin) may play a role in the decrease of

329   mean molecular weight of DOM along the stream.

330   Similar to $SUVA_{254}$ and $S_{275\text{-}295}$, the data from FT-ICR MS also show a downstream

331   decrease in aromaticity (AI_{mod}: 0.43 to 0.36) and mean molecular weight of stream

332   DOM (510.0 to 486.5 Da; Table 1). Compared with headstream DOM at Q-1, DOM at

333   Q-9 and Q-17 was characterized by a lower proportion of condensed aromatics and

334   polyphenols and enriched in highly unsaturated compounds (Table 1). The decrease in

335   relative abundance of aromatic compounds is consistent with the reports for the

336   photolability of aromatic formulas within permafrost, river and ocean DOM (Stubbins

337   and Dittmar, 2015; Stubbins et al., 2017).

338   As discussed in section 4.1, AL is the principal contributor to stream DOM. Thus,

339   tracing AL-derived DOM is paramount in estimating biogeochemical processes of

340   carbon in the stream. FT-ICR MS identified 6409 molecular formulas specific to AL-

341   leachates (i.e. not observed in the PL, Table 2). Through various stream processes, some

342   AL specific formulas were removed from the DOM pool (from 17% by Q-1 up to 59%

343   by Q-17), which accounted for 66% of the aromatic compounds and 51% of the highly

344   unsaturated compounds (Table 2). Molecular formulas containing N and/or S were more

345   labile in the fluvial networks than CHO formulas, with 84% of S-containing formulas

346   and 100% of S and N-containing formulas lost (Table 2). Furthermore, the removal of

347   DOM formulas (ca. 83% of AL-specific formulas, and >95% of AL-specific formulas)

348   occurred in upper and mid-stream (leachates to Q-9). Concurrent with the rapid loss of

349   AL-specific formulas, some new molecular formulas were detected by FT-ICR MS,

350   which was mainly attributed to in-situ production by stream algae/microbes, although

351   an import form groundwater could not be excluded. The addition of those new

352   molecular formulas was also reflected by the ^{14}C enrichment in middle and lower-

353   stream (Fig. 3b).

354   Overall, our multiple analyses demonstrate a rapid and selective degradation of

355   stream DOM on the QTP. The attenuation of aromatic compounds and enrichment of

356   highly unsaturated compounds could change the environmental photo- and bio-lability

357   of DOM, increasing relative importance of photodegradation in upper stream and

358   biodegradation in lower stream. The continuous change in chemical properties of DOM

359   along the alpine stream flowpath has a potential to shift the aquatic microbial

360   community since DOM serves as an important energy and nutrient source(Wild et al.,

361   2014).

362

363   **4.3. Prediction of in stream carbon dynamic under continued warming**

364   The DOC concentrations, UV-visible optical parameters and FT-ICR MS all suggest

365   that currently, PL is a minor source to stream DOM (see 4.1). However, the QTP is a

366   sensitive area to global warming, with a rate of air temperature rise that is

367   approximately three times the global warming rate (Qiu, 2008). According to climate

368   model predictions, spatial average temperatures of the QTP will increase by 0.68–0.98

369   ºC for the period of 2015–2050 (Zhu et al., 2013), and in 2050, the mean AL thickness

370   on the QTP permafrost will increase by approximately 0.3-0.8 m more than that in 2010

Biogeosciences
Discussions

Open Access

EGU

371   (Zhang and Wu, 2012). With the deepening of the AL, carbon that is currently stable in

372   the PL will be thawed and mobilized into the downslope aquatic environments, which

373   inevitably changes the proportion of AL vs. PL contributions to stream DOM. Thus, it

374   is worth to trace chemical change of PL leachates along the stream. The PL leachate

375   contained only 1345 formulas unique to the PL leachate in comparison to the AL,

376   accounting for 14% of total assigned formulas (Table 2). Most PL-specific formulas

377   were more biolabile components, e.g. aliphatics and peptides (73%), followed by highly

378   unsaturated formulas (23.6%) and aromatics (1.9%). At the downstream site (i.e., Q-

379   17), 90% of these PL-specific molecular formulas were lost, substantially higher than

380   that of AL-specific formulas (59%). Furthermore, the vast majority of PL-specific

381   formulas were lost within < 1 km (Q-1: 83%) whereas only 17% of AL-specific

382   formulas were lost by Q-1 (Table 2). Therefore, the FT-ICR MS data demonstrate that

383   permafrost thaw can trigger a rapid degradation of old carbon that was frozen in soils

384   for thousands of years (Fig. 3a). This is consistent with findings in Arctic fluvial

385   networks that show the utilization of ancient permafrost carbon in headstream waters

386   was rapid (Mann et al., 2015; Frey et al., 2016). Therefore, we hypothesize that with

387   enhanced leaching of deep soil C under continued warming on the QTP, DOM in alpine

388   streams will be more enriched in biolabile aliphatics/peptides and depleted in

389   photolabile aromatics

390   Finally, despite substantial in-stream degradation, some old permafrost-derived

391   carbon (i.e., polyphenols and highly unsaturated compounds) could persist downstream.

392   In addition, CO_2 produced by respiration of old DOC could be utilized by stream algae

393   to biosynthesize new DOM with an old carbon age. These effects resulted in a sustained

394   deviation from modern ^{14}C-DOC age in the alpine stream (e.g., 160 years BP at Q-19),

395   and were even detected in large rivers on the QTP (e.g., Yangtze River and Yellow River;

396   Qu et al., 2017). Thus, under continued warming, a greater quantity of older C may be

397   transported into large watersheds on the QTP, and thereby exert an important role in

398   biogeochemical cycles there since older carbon has different photo and bio-lability from

399   young carbon in AL soils.

400

401   **5. CONCLUSIONS**

402   Permafrost thaw represents positive feedbacks to climate change, but its carbon

403   alteration and removal mechanism is not well known, particularly for the alpine

404   permafrost such as the QTP. Here we use multiple analytical methods (e.g., FT-ICR MS,

405   radiocarbon and UV-visible spectroscopy) to trace spatial and temporal variability of

406   permafrost DOM along an alpine stream in the northeastern QTP, from which four

407   conclusions have been reached.

408   1)   Presently, the AL is the major source to stream DOM with relatively high

409   aromaticity. This character, combined with strong solar radiation on the QTP, suggests

410   sunlight may be an important driver for DOM removal in alpine fluvial networks, which

411   was corroborated by an almost 60% loss of AL specific formulas from the thermo-

412   erosion gully head to downstream waters.

413   2)   From summer to fall (seasonal permafrost thawing to freezing cycle), the

414   concentrations and chemical composition of stream DOM varied significantly at the

415   thermo-erosion gully head. Even though the total amount of the leached DOC decreased,

416   the contribution of deep permafrost carbon increased, reflected by an increase of ^{14}C-

417   DOC age and a decrease in aromaticity of DOM.

418   3)   Although both the AL and PL leachate DOM underwent rapid degradation in

419   the alpine stream, some components with old ^{14}C-DOC age (mainly highly unsaturated)

420   were recalcitrant to degradation and could be transported downstream, causing ^{14}C-

17

421   DOC values that were more depleted than modern radiocarbon age downstream in our

422   study, and even in large watersheds as observed in Qu et al. (2017).

423   4) With deepening of the AL under continued climate warming on the QTP,

424   currently stable PL soils will thaw and release greater amounts of old, aliphatic/peptide-

425   rich DOM to downstream waters. This change in source and chemical composition will

426   make microbial degradation more important for carbon removal and may shift

427   downstream microbial communities, even in large watershed systems. All these factors

428   should be taken into account when interpreting alpine permafrost carbon dynamics

429   under the amplified climate warming trend on the QTP.

430

431   **ACKNOWLEDGEMENTS**

437

438

439   **References**

440   Abbott, B.W., Jones, J.B., Godsey, S.E., Larouche, J.R. and Bowden, W.B. (2015)

441   Patterns and persistence of hydrologic carbon and nutrient export from collapsing

442   upland permafrost. Biogeosciences 12, 3725-3740.

443   Aiken, G.R., Spencer, R.G.M., Striegl, R.G., Schuster, P.F. and Raymond, P.A. (2014)

444   Influences of glacier melt and permafrost thaw on the age of dissolved organic carbon

445   in the Yukon River basin. Global Biogeochem. Cycles 28, 525-537.

446   Amon, R.M.W. and Benner, R. (1996) Bacterial utilization of different size classes of

447   dissolved organic matter. Limnol. Oceanogr. 41, 41-51.

448   Bockheim, J.G. and Munroe, J.S. (2014) Organic Carbon Pools and Genesis of Alpine

449   Soils with Permafrost: A Review. Arct. Antarct. Alp. Res. 46, 987-1006.

450   Corilo, Y.E. (2015) EnviroOrg. Florida State University.

451   Cory, R.M., Crump, B.C., Dobkowski, J.A. and Kling, G.W. (2013) Surface exposure

452   to sunlight stimulates CO_2 release from permafrost soil carbon in the Arctic. Proc. Natl.

453   Acad. Sci. USA 110, 3429-3434.

454   Cory, R.M., Ward, C.P., Crump, B.C. and Kling, G.W. (2014) Sunlight controls water

455   column processing of carbon in arctic fresh waters. Science 345, 925-928.

456   Criss, R.E. (1999) Principles of stable isotope distribution. Oxford University Press,

457   New York.

458   Dittmar, T., Koch, B., Hertkorn, N. and Kattner, G. (2008) A simple and efficient

459   method for the solid-phase extraction of dissolved organic matter (SPE-DOM) from

460   seawater. Limnol. Oceanogr. Methods 6, 230-235.

461   Drake, T.W., Wickland, K.P., Spencer, R.G., McKnight, D.M. and Striegl, R.G. (2015)

462   Ancient low-molecular-weight organic acids in permafrost fuel rapid carbon dioxide

463   production upon thaw. Proc. Natl. Acad. Sci. USA 112, 13946-13951.

464   Fichot, C.G. and Benner, R. (2012) The spectral slope coefficient of chromophoric

465   dissolved organic matter ($S_{275-295}$) as a tracer of terrigenous dissolved organic carbon

466   in river-influenced ocean margins. Limnol. Oceanogr. 57, 1453-1466.

467   Frey, K.E. and Smith, L.C. (2005) Amplified carbon release from vast West Siberian

468   peatlands by 2100. Geophys. Res. Lett. 32, doi: 10.1029/2004GL022025.

469   Frey, K.E., Sobczak, W.V., Mann, P.J. and Holmes, R.M. (2016) Optical properties and

470   bioavailability of dissolved organic matter along a flow-path continuum from soil pore

Biogeosciences
Discussions

Open Access

EGU

471   waters to the Kolyma River mainstem, East Siberia. Biogeosciences 13, 2279-2290.

472   Ge, S., Wu, Q.B., Lu, N., Jiang, G.L. and Ball, L. (2008) Groundwater in the Tibet

473   Plateau, western China. Geophys. Res. Lett. 35, 80-86.

474   Hedges, J.I., Cowie, G.L., Ertel, J.R., James Barbour, R. and Hatcher, P.G. (1985)

475   Degradation of carbohydrates and lignins in buried woods. Geochim. Cosmochim. Acta

476   49, 701-711.

477   Hedges, J.I., Keil, R.G. and Benner, R. (1997) What happens to terrestrial organic

478   matter in the ocean? Org. Geochem. 27, 195-212.

479   Helms, J.R., Stubbins, A., Ritchie, J.D., Minor, E.C., Kieber, D.J. and Mopper, K. (2008)

480   Absorption spectral slopes and slope ratios as indicators of molecular weight, source,

481   and photobleaching of chromophoric dissolved organic matter. Limnol. Oceanogr. 53,

482   955-969.

483   Hodgkins, S.B., Tfaily, M.M., Podgorski, D.C., Mccalley, C.K., Saleska, S.R., Crill,

484   P.M., Rich, V.I., Chanton, J.P. and Cooper, W.T. (2016) Elemental composition and

485   optical properties reveal changes in dissolved organic matter along a permafrost thaw

486   chronosequence in a subarctic peatland. Geochim. Cosmochim. Acta 187, 123-140.

487   Kaiser, N.K., Quinn, J.P., Blakney, G.T., Hendrickson, C.L. and Marshall, A.G. (2011)

488   A novel 9.4 tesla FTICR mass spectrometer with improved sensitivity, mass resolution,

489   and mass range. J. Am. Soc. Mass Spectrom. 22, 1343-1351.

490   Kang, S., Xu, Y., You, Q., Flügel, W.-A., Pepin, N. and Yao, T. (2010) Review of climate

491   and cryospheric change in the Tibetan Plateau. Environ. Res. Lett. 5, doi:10.1088/1748-

492   9326/1085/1081/015101.

493   Kellerman, A.M., Guillemette, F., Podgorski, D.C., Aiken, G.R., Butler, K.D. and

494   Spencer, R.G.M. (2018) Unifying Concepts Linking Dissolved Organic Matter

495   Composition to Persistence in Aquatic Ecosystems. Environ. Sci. Technol., doi:

496   10.1021/acs.est.1027b05513.

497   Kellerman, A.M., Kothawala, D.N., Dittmar, T. and Tranvik, L.J. (2015) Persistence of

498   dissolved organic matter in lakes related to its molecular characteristics. Nat. Geosci. 8,

499   454-457.

500   Koch, B.P. and Dittmar, T. (2006) From mass to structure: an aromaticity index for high-

501   resolution mass data of natural organic matter. Rapid Commun. Mass Spectrom. 20,

502   926-932.

503   Koven, C.D., Ringeval, B., Friedlingstein, P., Ciais, P., Cadule, P., Khvorostyanov, D.,

504   Krinner, G. and Tarnocai, C. (2011) Permafrost carbon-climate feedbacks accelerate

505   global warming. Proc. Natl. Acad. Sci. U. S. A. 108, 14769-14774.

506   Lanzalunga, O. and Bietti, M. (2000) Photo- and radiation chemical induced

507   degradation of lignin model compounds. J. Photochem. Photobiol. B: Biol. 56, 85-108.

508   Laudon, H., Berggren, M., Ågren, A., Buffam, I., Bishop, K., Grabs, T., Jansson, M.

509   and Köhler, S. (2011) Patterns and dynamics of dissolved organic carbon (DOC) in

510   boreal streams: the role of processes, connectivity, and scaling. Ecosystems 14, 880-

511   893.

512   Mann, P.J., Davydova, A., Zimov, N., Spencer, R.G.M., Davydov, S., Bulygina, E.,

513   Zimov, S. and Holmes, R.M. (2012) Controls on the composition and lability of

514   dissolved organic matter in Siberia's Kolyma River basin. J. Geophys. Res. Biogeosci.

515   117, doi:10.1029/2011jg001798.

516   Mann, P.J., Eglinton, T.I., McIntyre, C.P., Zimov, N., Davydova, A., Vonk, J.E., Holmes,

517   R.M. and Spencer, R.G. (2015) Utilization of ancient permafrost carbon in headwaters

518   of Arctic fluvial networks. Nat. Commun. 6, doi:10.1038/ncomms8856.

519   Mu, C., Zhang, T., Zhang, X., Li, L., Guo, H., Zhao, Q., Cao, L., Wu, Q. and Cheng, G.

520   (2016) Carbon loss and chemical changes from permafrost collapse in the northern

521   Tibetan Plateau. J. Geophys. Res. Biogeosci. 121, doi:10.1002/2015JG003235.

522   O'Donnell, J.A., Aiken, G.R., Walvoord, M.A., Raymond, P.A., Butler, K.D.,

523   Dornblaser, M.M. and Heckman, K. (2014) Using dissolved organicmatter age and

524   composition to detect permafrost thaw in boreal watersheds of interior Alaska. J.

525   Geophys. Res. Biogeosci. 119, 2155-2170.

526   Peng, S., Du, Q., Wang, L., Lin, A. and Hu, B. (2015) Long-term variations of

527   ultraviolet radiation in Tibetan Plateau from observation and estimation. Int. J. Climatol.

528   35, 1245-1253.

529   Petrone, K.C., Jones, J.B., Hinzman, L.D. and Boone, R.D. (2006) Seasonal export of

530   carbon, nitrogen, and major solutes from Alaskan catchments with discontinuous

531   permafrost. J. Geophys. Res. Biogeosci. 111, doi:10.1029/2006JG000281.

532   Qiu, J. (2008) The third pole. Nature 454, 393-396.

533   Qu, B., Sillanpää, M., Li, C., Kang, S., Stubbins, A., Yan, F., Aho, K.S., Zhou, F. and

534   Raymond, P.A. (2017) Aged dissolved organic carbon exported from rivers of the

535   Tibetan   Plateau.   PLoS   One   12,   e0178166,   doi:

536   0178110.0171371/journal.pone.0178166.

537   Sato, T. and Kimura, F. (2007) How does the Tibetan Plateau affect the transition of

538   Indian monsoon rainfall? Mon. Weather Rev. 135, 2006-2015.

539   Schuur, E.A.G., McGuire, A.D., Schadel, C., Grosse, G., Harden, J.W., Hayes, D.J.,

540   Hugelius, G., Koven, C.D., Kuhry, P., Lawrence, D.M., Natali, S.M., Olefeldt, D.,

541   Romanovsky, V.E., Schaefer, K., Turetsky, M.R., Treat, C.C. and Vonk, J.E. (2015)

542   Climate change and the permafrost carbon feedback. Nature 520, 171-179.

543   Selvam, B.P., Lapierre, J.-F., Guillemette, F., Voigt, C., Lamprecht, R.E., Biasi, C.,

544   Christensen, T.R., Martikainen, P.J. and Berggren, M. (2017) Degradation potentials of

545   dissolved organic carbon (DOC) from thawed permafrost peat. Sci. Rep. 7,

Biogeosciences
Discussions

Open Access

EGU

546   doi:10.1038/srep45811.

547   Spencer, R.G., Aiken, G.R., Wickland, K.P., Striegl, R.G. and Hernes, P.J. (2008)

548   Seasonal and spatial variability in dissolved organic matter quantity and composition

549   from the Yukon River basin, Alaska. Global Biogeochem. Cycles 22, doi:

550   10.1029/2008GB003231.

551   Spencer, R.G.M., Aiken, G.R., Butler, K.D., Dornblaser, M.M., Striegl, R.G. and

552   Hernes, P.J. (2009) Utilizing chromophoric dissolved organic matter measurements to

553   derive export and reactivity of dissolved organic carbon exported to the Arctic Ocean:

554   a case study of the Yukon River, Alaska. Geophys. Res. Lett. 36, 141-153.

555   Spencer, R.G.M., Guo, W., Raymond, P.A., Dittmar, T., Hood, E., Fellman, J. and

556   Stubbins, A. (2014) Source and biolability of ancient dissolved organic matter in glacier

557   and lake ecosystems on the Tibetan Plateau. Geochim. Cosmochim. Acta 142, 64-74.

558   Striegl, R.G., Dornblaser, M.M., Aiken, G.R., Wickland, K.P. and Raymond, P.A. (2007)

559   Carbon export and cycling by the Yukon, Tanana, and Porcupine rivers, Alaska, 2001–

560   2005. Water Resour. Res. 43, doi:10.1029/2006WR005201.

561   Stubbins, A. and Dittmar, T. (2015) Illuminating the deep: Molecular signatures of

562   photochemical alteration of dissolved organic matter from North Atlantic Deep Water.

563   Mar. Chem. 177, 318-324.

564   Stubbins, A., Mann, P.J., Powers, L., Bittar, T.B., Dittmar, T., McIntyre, C.P., Eglinton,

565   T.I., Zimov, N. and Spencer, R.G.M. (2017) Low photolability of yedoma permafrost

566   dissolved organic carbon. J. Geophys. Res. Biogeosci. 122, 200-211.

567   Stubbins, A., Spencer, R.G.M., Chen, H.M., Hatcher, P.G., Mopper, K., Hernes, P.J.,

568   Mwamba, V.L., Mangangu, A.M., Wabakanghanzi, J.N. and Six, J. (2010) Illuminated

569   darkness: Molecular signatures of Congo River dissolved organic matter and its

570   photochemical alteration as revealed by ultrahigh precision mass spectrometry. Limnol.

Biogeosciences
Discussions

Open Access

EGU

571   Oceanogr. 55, 1467-1477.

572   Stuiver, M. and Reimer, P.J. (1993) Extended ^{14}C Data Base and Revised Calib 3. 0 14C

573   Age Calibration Program. Radiocarbon 35, 215-230.

574   Tarnocai, C., Canadell, J.G., Schuur, E.A.G., Kuhry, P., Mazhitova, G. and Zimov, S.

575   (2009) Soil organic carbon pools in the northern circumpolar permafrost region. Global

576   Biogeochem. Cycles 23, doi:10.1029/2008gb003327.

577   Vonk, J.E., Mann, P.J., Davydov, S., Davydova, A., Spencer, R.G.M., Schade, J.,

578   Sobczak, W.V., Zimov, N., Zimov, S., Bulygina, E., Eglinton, T.I. and Holmes, R.M.

579   (2013) High biolability of ancient permafrost carbon upon thaw. Geophys. Res. Lett.

580   40, 2689-2693.

581   Vonk, J.E., Tank, S.E., Bowden, W.B., Laurion, I., Vincent, W.F., Alekseychik, P.,

582   Amyot, M., Billet, M.F., Canario, J., Cory, R.M., Deshpande, B.N., Helbig, M., Jammet,

583   M., Karlsson, J., Larouche, J., MacMillan, G., Rautio, M., Anthony, K.M.W. and

584   Wickland, K.P. (2015) Reviews and syntheses: Effects of permafrost thaw on Arctic

585   aquatic ecosystems. Biogeosciences 12, 7129-7167.

586   Wang, B., Bao, Q., Hoskins, B., Wu, G. and Liu, Y. (2008) Tibetan Plateau warming

587   and precipitation changes in East Asia. Geophys. Res. Lett. 35, 63-72.

588   Ward, C.P. and Cory, R.M. (2016) Complete and Partial Photo-oxidation of Dissolved

589   Organic Matter Draining Permafrost Soils. Environ. Sci. Technol. 50, 3545-3553.

590   Weishaar, J.L., Aiken, G.R., Bergamaschi, B.A., Fram, M.S., Fujii, R. and Mopper, K.

591   (2003) Evaluation of specific ultraviolet absorbance as an indicator of the chemical

592   composition and reactivity of dissolved organic carbon. Environ. Sci. Technol. 37,

593   4702-4708.

594   Wickland, K.P., Aiken, G.R., Butler, K., Dornblaser, M.M., Spencer, R.G.M. and Striegl,

595   R.G. (2012) Biodegradability of dissolved organic carbon in the Yukon River and its

596   tributaries: Seasonality and importance of inorganic nitrogen. Global Biogeochem.

597   Cycles 26, doi:10.1029/2012GB004342.

598   Wild, B., Schnecker, J., Alves, R.J.E., Barsukov, P., Bárta, J., Čapek, P., Gentsch, N.,

599   Gittel, A., Guggenberger, G., Lashchinskiy, N., Mikutta, R., Rusalimova, O.,

600   Šantrůčková, H., Shibistova, O., Urich, T., Watzka, M., Zrazhevskaya, G. and Richter,

601   A. (2014) Input of easily available organic C and N stimulates microbial decomposition

602   of soil organic matter in arctic permafrost soil. Soil Biol. Biochem. 75, 143-151.

603   Wu, G., Liu, Y., Zhang, Q., Duan, A., Wang, T., Wan, R., Liu, X., Li, W., Wang, Z. and

604   Liang, X. (2007) The influence of mechanical and thermal forcing by the Tibetan

605   Plateau on Asian climate. J. Hydrometeorol. 8, 770-789.

606   Yao, T., Pu, J., Lu, A., Wang, Y. and Yu, W. (2007) Recent glacial retreat and its impact

607   on hydrological processes on the Tibetan Plateau, China, and surrounding regions. Arct.

608   Antarct. Alp. Res. 39, 642-650.

609   Zhang, Z.Q. and Wu, Q.-B. (2012) Predicting changes of active layer thickness on the

610   Qinghai-Tibet Plateau as climate warming. J. Glaciol. Geocryol. 34, 505-511.

611   Zhu, X., Wang, W. and Fraedrich, K. (2013) Future climate in the Tibetan Plateau from

612   a statistical regional climate model. J. Clim. 26, 10125-10138.

613   Zimov, S.A., Schuur, E.A.G. and Chapin, F.S. (2006) Permafrost and the global carbon

614   budget. Science 312, 1612-1613.

615

616

617 **Figure and table captions**

618 **Fig. 1.** Location of the QTP and sampling sites Q1 to Q20. Sites marked by a star were
619 selected for FT-ICR MS and ^{14}C-DOC analyses. The AL and PL denote the sampling
620 locations of the active and permafrost layers. The blue line and the red line represent
621 the first order and second order stream, respectively, and the blue dashed line denotes
622 stream without GPS data.

623 **Fig. 2.** (a) Stream water discharge, (b) pH, and (c) conductivity at the sampling sites in
624 2015; and (d) DOC concentration in stream water and PL/AL leachates collected in
625 2015 (filled circles) and 2016 (open circles).

626 **Fig. 3.** UV-visible optical indices of the stream water and PL/AL leachate samples
627 collected in 2015 (filled circles) and 2016 (open circles) on the QTP: $S_{275-295}$ (a) and
628 SUVA$_{254}$ (b).

629 **Fig. 4.** Variations of ^{14}C-DOC age across the alpine stream spatially (a), and at
630 headstream Q-1 temporally (b).

631 **Fig. 5.** van Krevelen diagrams of AL leachate DOM (a), PL leachate DOM (b),
632 headstream DOM Q-1 (c), downstream DOM Q-17 (d), the relative abundance of
633 defined compound class in different samples (e). CA = condensed aromatics, Pol. =
634 polyphenols, Uns. = highly unsaturated compounds, Ali. = aliphatics, Pep. = peptides;
635 and Sug. = Sugar.

636 **Fig. 6.** (a) Relative contribution of AL leachate DOM to headstream DOM (Q-1); and
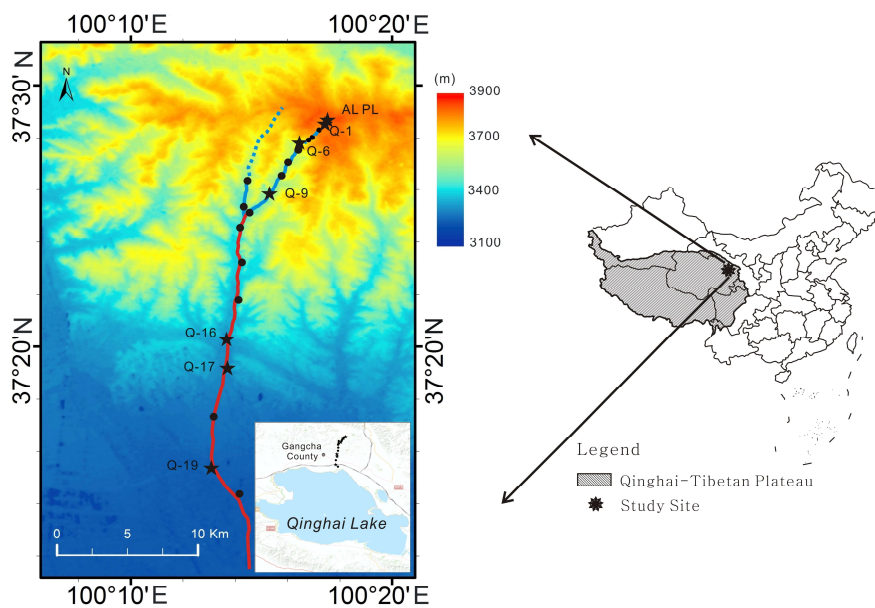637 (b) temporal variation of the DOC concentration at headstream Q-1.

638 **Table 1** The number of molecular formulas assigned, modified aromaticity index
639 (AI$_{mod}$), mean molecular weight (mean MW) and relative abundance of defined
640 compound classes detected by FT-ICR MS for DOM samples from the QTP, including
641 soil leachates (AL and PL) and stream waters (Q-1, Q-9 and Q-17). CA = condensed
642 aromatics, Pol. = polyphenols, Uns. = highly unsaturated compounds, Ali. = aliphatic,
643 Pep. = peptides.

644 **Table 2** The number of specific molecules identified in the AL leachate DOM and the
645 PL leachate DOM within the fluvial network, and the percentage of peaks totally
646 degraded during the transportation.
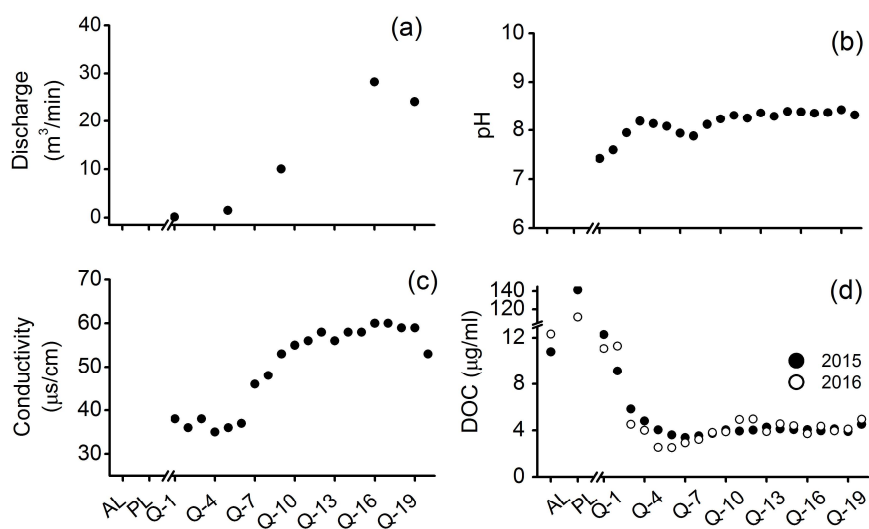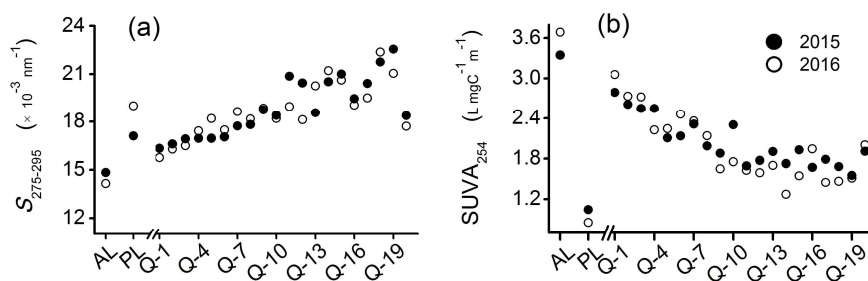
647

648   Fig. 1

649
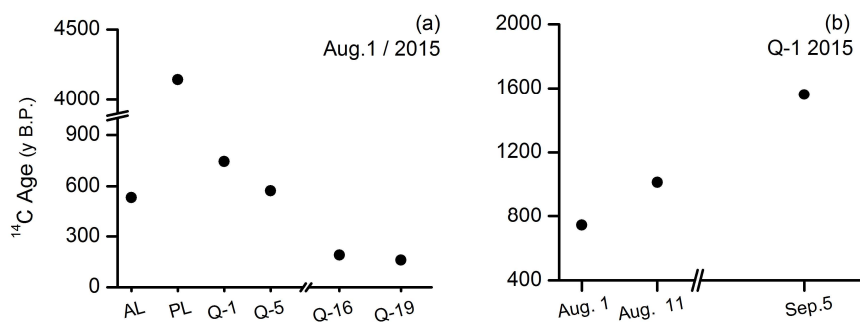
650

651   Fig. 2

652

653

654   Fig. 3

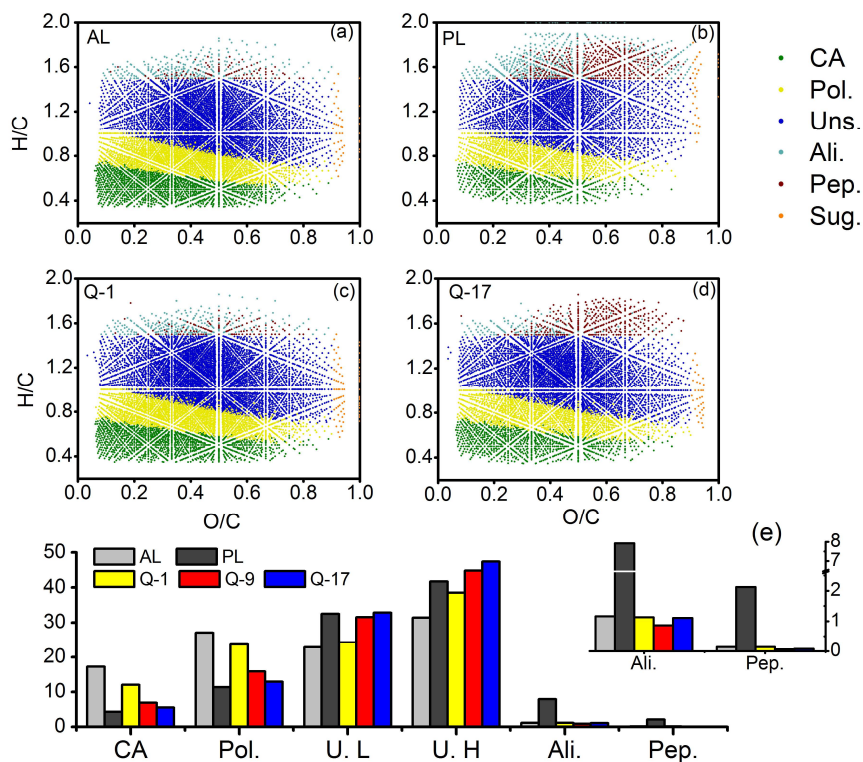657   Fig. 4

658

659

660   Fig. 5
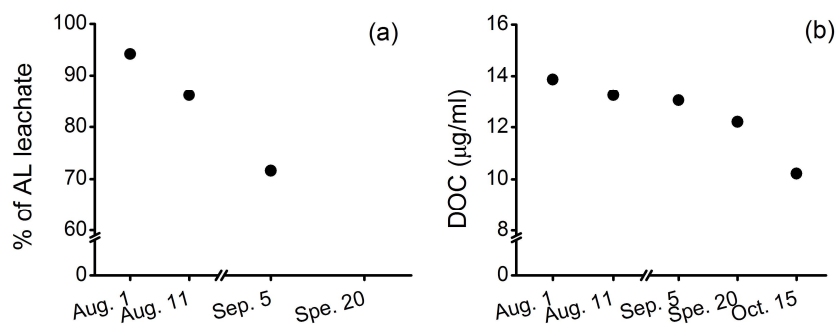

661

662

663 Fig. 6

664

665

Biogeosciences
Discussions

Open Access

EGU

666 **Table 1.** The number of molecular formulas assigned, modified aromaticity index
667 (AI$_{mod}$), mean molecular weight (mean MW) and relative abundance of defined
668 compound classes detected by FT-ICR MS for DOM samples from the QTP, including
669 soil leachates (AL and PL) and stream waters (Q-1, Q-9 and Q-17). CA = condensed
670 aromatics, Pol. = polyphenols, Uns. = highly unsaturated compounds, Ali. = aliphatic,
671 Pep. = peptides.
672

Sample	Formulas assigned	Mean MW	AI$_{mod}$	CA (%)	Pol. (%)	Uns. (%)	Ali. (%)	Pep. (%)
AL	14709	498.81	0.47	17.23	27.10	54.28	1.16	0.14
PL	9645	452.73	0.30	4.32	11.33	74.23	7.92	2.12
Q-1	14924	510.07	0.43	12.05	23.69	62.85	1.14	0.14
Q-9	11724	500.19	0.38	6.86	15.82	76.32	0.86	0.06
Q-17	11074	486.50	0.36	5.53	12.91	80.31	1.11	0.08

673

674

Table 2: The number of specific molecules identified in the AL leachate DOM and the PL leachate DOM within the fluvial network, and the percentage of peaks totally degraded during the transportation.

Samples		All peaks	Only CHO	Contains N	Contains S	Contains N& S	Condensed aromatics	Polyhoenols	Unsatuated	Aliphatics	Peptides
	AL	6409	1793	3370	424	822	1620	1720	2970	38	23
AL specific	Q-1	5311 (17%)	1653 (8%)	2791 (17%)	349 (18%)	517 (37%)	1278 (21%)	1416 (18%)	2549 (14%)	20 (47%)	14 (39%)
	Q-9	3365 (47%)	1294 (28%)	1917 (43%)	153 (64%)	0 (100%)	748 (54%)	838 (51%)	1759 (41%)	6 (84%)	1 (96%)
	Q-17	2623 (59%)	985 (45%)	1570 (53%)	67 (84%)	0 (100%)	550 (66%)	602 (65%)	1453 (51%)	5 (87%)	0 (100%)
	PL	1345	515	551	278	0	2	23	318	597	385
PL specific	Q-1	222 (83%)	90 (83%)	102 (81%)	30 (89%)	0	0 (100%)	11 (52%)	126 (60%)	46 (92%)	36 (91%)
	Q-9	117 (91%)	44 (91%)	46 (92%)	27 (90%)	0	2 (0%)	14 (39%)	96 (70%)	1 (100%)	4 (99%)
	Q-17	130 (90%)	47 (91%)	55 (90%)	28 (90%)	0	2 (0%)	13 (43%)	104 (67%)	6 (99%)	5 (99%)